Incorporating a hydrophobic solid into a coarse grain liquid framework: Graphite in an aqueous amphiphilic environment

Steven O. Nielsen, Goundla Srinivas, and Michael L. Klein[a)]
Center for Molecular Modeling, Department of Chemistry, University of Pennsylvania, Philadelphia, Pennsylvania 19104-6323

(Received 9 May 2005; accepted 5 July 2005; published online 26 September 2005)

A method is presented for incorporating a solid into a coarse grain liquid model. From the fully atomistic solid-liquid site-site description the solid is replaced by an implicit potential. The liquid particles are then coarse grained by appealing to statistical mechanics and probability theory. The dimensionality problem which arises is overcome with an approximate treatment and a force field is derived for graphite interacting with an existing coarse grain liquid model. Water is considered separately by using the experimentally observed contact angle between a water droplet and a graphite surface. Finally, the solid is restored to an explicit representation to allow for different geometries. © *2005 American Institute of Physics*. [DOI: 10.1063/1.2009734]

I. INTRODUCTION

Coarse grain models constitute one component in the arsenal deployed by the simulation community against the usual adversary of length and time scales.[1] Many coarse grain (CG) liquid models are being developed for and applied to a range of biological, polymer, and material problems.[2–8] However, at present no coarse grain method has been proposed to describe a solid-liquid interface. The range of study would be greatly extended with the introduction of such an interface.[9,10] For example, two problems of current interest in the field of amphiphilic self-assembly are the aggregation morphology of surfactants at a flat graphite-liquid interface[11] and the adsorption of surfactants on carbon nanotubes in an effort to make stable suspensions of individual nanotubes.[12]

In what follows we develop a general strategy for incorporating a solid into a CG liquid framework and apply it to the specific case of adding graphite to an existing aqueous amphiphilic CG model.[13,14] Recently, we gave a brief account of this method.[15] Our starting point is the fully atomistic description of a gas or liquid particle interacting with an individual site in the solid, and its reduction to the interaction of this particle with the entire solid through an implicit potential (Sec. II). The implicit representation allows for the liquid particles to be rigorously coarse grained by appealing to probability theory (Secs. III and IV A). The dimensionality problem which arises is overcome (Sec. IV B) and the entire approach is applied to the case of graphite interacting with an existing amphiphilic CG model (Sec. V). In Sec. VI the CG water-graphite parameters are derived following the recent atomistic study by Werder *et al.*[16] Finally, the implicit description is undone to recover the fully CG liquid-graphite site-site parameters (Sec. VII).

II. ATOMISTIC AND IMPLICIT GRAPHITE REPRESENTATIONS

Atomistic studies of the liquid-solid interface rarely use a site-site description because of the computational cost this would entail. Instead, the sites in the solid are integrated over to leave the liquid particles in the presence of an implicit potential. In the simplest such implicit description the potential experienced by the liquid particles depends only on their height above the surface. The standard derivation of this implicit potential is as follows.[17] Suppose that an individual site in the surface interacts with a particle in the gas or liquid phase via a 12-6 Lennard-Jones potential,

$$u(r) = 4\epsilon\left[\left(\frac{\sigma}{r}\right)^{12} - \left(\frac{\sigma}{r}\right)^{6}\right]. \tag{1}$$

The solid is approximated as a continuum with number density $\rho = N/V$ that occupies the semi-infinite region $z \leqslant 0$. A particle at height $z > 0$ interacts with the solid as

$$\int_z^\infty dr \int_0^{2\pi} d\theta \int_{\pi-\cos^{-1}(z/r)}^{\pi} d\phi r^2 \sin\phi \rho u(r) = \frac{4}{45}\frac{\pi\rho\epsilon\sigma^{12}}{z^9} - \frac{2}{3}\frac{\pi\rho\epsilon\sigma^6}{z^3} \equiv U(z). \tag{2}$$

Such a description has been used by Lee and Rossky,[18] and by Shelley and Patey.[19] More sophisticated implicit descriptions exist which account for corrugation by including periodic functions in the directions parallel to the surface. This is a minor effect: Hentschke *et al.*[20] showed that, for $C_{24}H_{50}$ physisorbed on graphite, the potential in the direction perpendicular to the graphite surface varies by 40 kcal/mol from infinite separation to the bottom of the attractive well, while the potential varies by roughly 1 kcal/mol in the directions parallel to the surface. The simple description of Eq. (2) suffices for our purposes. First, since we will eventually undo the implicit representation to return to an explicit site description of the surface (see Sec. VII), the implicit representation can be thought of merely as an intermediate com-

[a)]URL: www.cmm.upenn.edu; Electronic mail: snielsen@cmm.upenn.edu

putational aid. Second, the effect of corrugation is small and in the spirit of coarse graining this level of detail may not be deemed necessary. On the other hand, it will become clear in what follows that the representation of the surface is the least expensive part of the overall method in terms of computational cost. This is because the surface-liquid interactions are one dimensional and are only computed once. Hence a more accurate surface representation could be used with almost no added computational cost. Possibilities include the extremely detailed representation used by Krishnan and Balasubramanian[21] and the clever hybrid representation discussed by Crowell.[22]

III. COARSE GRAINING TWO LIQUID PARTICLES

A coarse grain site consists of a single particle representing a collection of atomic sites. Given the potential experienced by one particle [Eq. (2)], we wish to derive the effective potential experienced by the center of mass of a collection of particles, corresponding to a coarse grain site. To realize this aim we move from describing interactions in terms of potential energies to describing them with probability distributions. The probability and the potential are related by $\mathcal{P}=e^{-\beta U}$. Note that the usual normalization problem exists (in analogy to radial distribution functions): we demand that the probability goes to unity at infinite separation.

We begin with the simplest case of two identical noninteracting particles. It is straightforward to remove this restriction and to consider different particles of unequal mass. This will be seen in Sec. V A but unnecessarily clutters the exposition presented here. The joint probability of finding particle 1 at height z_1 and particle 2 at height z_2 above the surface is given by

$$\mathcal{P}(z_1,z_2) = e^{-\beta U(z_1)}e^{-\beta U(z_2)}, \tag{3}$$

since the individual surface-particle potentials are additive. The probability of the center of mass being at height z is given by

$$\mathcal{P}(z_1+z_2=2z) = (2z)^{-1}\int_0^{2z} e^{-\beta U(z_1)}e^{-\beta U(2z-z_1)}dz_1. \tag{4}$$

The resulting potential is shown in Fig. 1. A temperature of 303.15 K is used for all of the results shown.

For two identical interacting particles the joint probability distribution is given by

$$\mathcal{P}(z_1,z_2) = e^{-\beta U(z_1)}e^{-\beta U(z_2)}\mathcal{P}_I(z_1,z_2). \tag{5}$$

The joint distribution is the product of three terms since the corresponding potential is composed of the sum of two particle-surface terms and an interaction term between the particles which does *not* involve the surface. The independence of the interaction term from the solid surface stems from the use of effective two-body forces in condensed matter atomistic force fields. For situations in which nonpairwise additive interactions are important, this procedure is not appropriate.

The interaction between two particles depends solely on their separation, $\mathcal{P}(r)\equiv\mathcal{P}_r(r)$, but we are asked to calculate the distribution as a function of the vertical separation of the particles. The conceptually simpler $\mathcal{P}_r(r)$ is either constructed from a (surface-free) simulation or by directly converting the potential between the particles (typically of harmonic form if the interaction is a chemical bond) into a probability distribution via $\mathcal{P}=e^{-\beta U}$. From this we integrate to obtain $\mathcal{P}_z(z)=\int dx\int dy\mathcal{P}_r(r)$, which is conveniently performed using cylindrical polar coordinates (R,θ,z)

$$\mathcal{P}_z(z) = \int_0^\infty dRR\mathcal{P}_r(\sqrt{R^2+z^2}). \tag{6}$$

The two distributions, $\mathcal{P}(r)$ and $\mathcal{P}(z)$, are shown in Fig. 2. Returning to Eq. (5), we may formulate the probability of the center of mass being at height z as

$$\mathcal{P}(z_1+z_2=2z) = \frac{\int_0^{2z} e^{-\beta U(z_1)}e^{-\beta U(2z-z_1)}\mathcal{P}_I(2z_1-2z)dz_1}{\int_0^{2z}\mathcal{P}_I(2z_1-2z)dz_1}, \tag{7}$$

where the normalization constant is the numerator with $U\equiv 0$, namely, with no surface. This probability distribution is

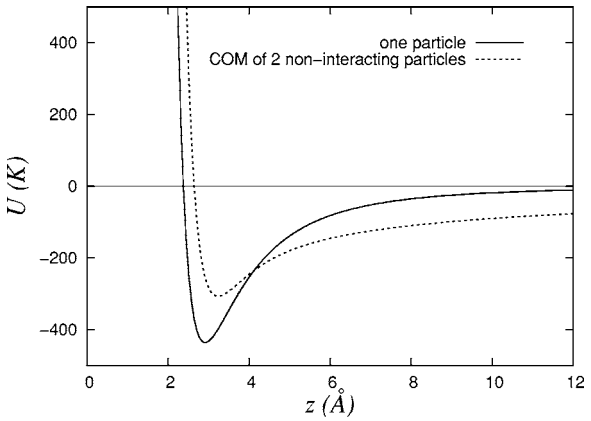

FIG. 1. Comparison of the potential experienced by a single particle at height z above a graphite surface, and the potential experienced by the center of mass of two noninteracting particles. See Eqs. (2) and (4) with $\epsilon=50$ K, $\sigma=3.3$ Å, and $\rho=0.113$ Å^{-3}. A temperature of 303.15 K is used for this plot and for all the other results shown.

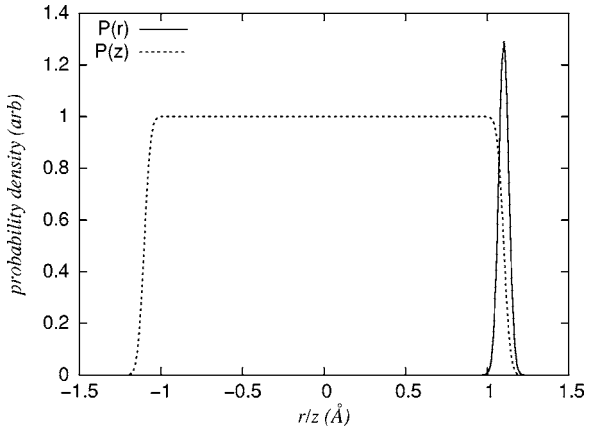

FIG. 2. The distributions $\mathcal{P}(r)$ and $\mathcal{P}(z)$ [see Eq. (6)] for two bonded particles with a harmonic bond of $k=311\,000$ K Å^{-2} and $r_{eq}=1.1$ Å. The distributions are not normalized.

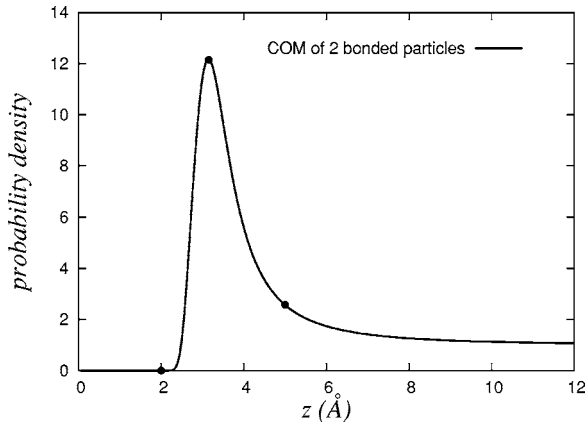

FIG. 3. The probability distribution for the center of mass of two bonded particles interacting with the surface [see Eq. (7)]. A harmonic potential with $k=500\,000$ K Å^{-2} and $r_{eq}=1.3$ Å is used. The distribution is normalized to be unity at infinite separation.

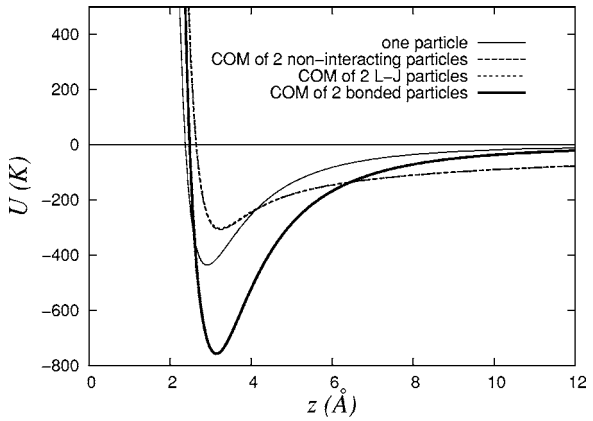

FIG. 4. Comparison of the potential one particle feels, and the effective potential that the center of mass of two noninteracting particles, two Lennard-Jones particles, and two bonded particles feel. The Lennard-Jones interaction is weak compared to the surface energy and is indistinguishable from the noninteracting case. For a nonbonded interaction, we take the Lennard-Jones 12-6 potential with $\epsilon=40$ and $\sigma=3.56$, which is typical for the interaction of two carbon atoms in the CHARMM force field. For a bonded interaction, we use a harmonic potential with $k=500\,000$ K Å^{-2} and $r_{eq}=1.3$ Å, which is also typical for the CHARMM force field. See Figs. 4, 3, and 5.

shown in Fig. 3 and the corresponding potential is shown in Fig. 4. The calculation of the values of the distribution at the marked points in Fig. 3 is shown in detail in Fig. 5 by plotting the three underlying probability distributions constituting Eqs. (5) and (7). In Eqs. (4) and (7) we performed the integration over the z coordinate of the first particle, having first eliminated the z coordinate of the second particle by using the center-of-mass constraint $z_2=2z-z_1$. The interaction term $\mathcal{P}_I(z_1,z_2)$ is equal to $\mathcal{P}_I(z_1-z_2)=\mathcal{P}_I(2z_1-2z)$ up to a normalization constant which cancels in the numerator and denominator of Eq. (7). These considerations result in the two individual particle-surface terms being reflections of one another in the line $z_1=z$ for a fixed center-of-mass value z (see Fig. 5). In addition, the interaction term from Fig. 2

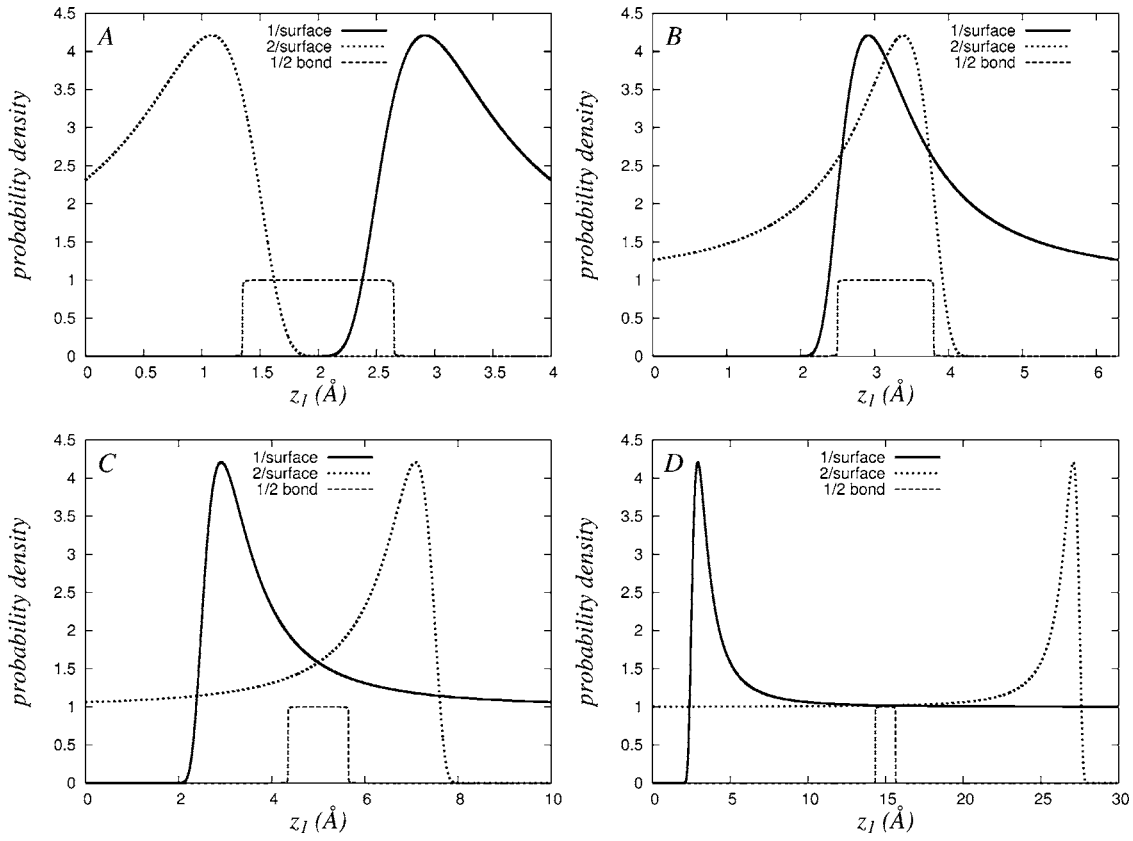

FIG. 5. The probability distribution for a fixed center-of-mass value z of two bonded particles interacting with the surface from Eq. (7). We show the integrand in the numerator broken down into its three constituent terms for four values of z (2.0, 3.15, 5.0, 15.0), where we have normalized the interaction term to have unit height since the denominator in Eq. (7) corrects for this arbitrary choice. The bond constrains the two particles to reside close to the center of mass. The overlap of this constraint with the surface interactions determines the net probability. Panels A, B, and C correspond to the three marked points of Fig. 3.

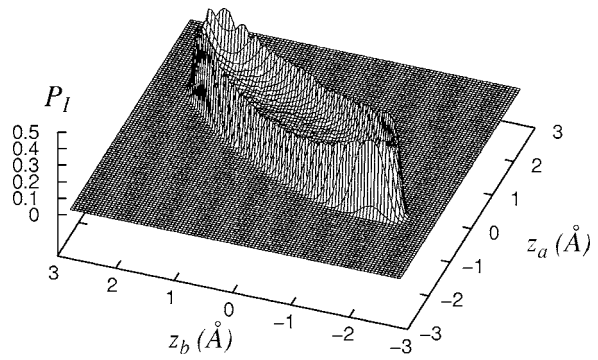

FIG. 6. The probability distribution of the relative coordinates (z_a, z_b) of a three-particle molecule with two bonds and a bend. This distribution selects a window from the individual particle-surface interaction terms in an analogous manner to the one-dimensional rectangular patch. We take typical values for carbon of $k=500\,000$ K Å^{-2} and $r_{eq}=1.3$ Å for the bonds and $k=50\,000$ K rad^{-2} and $\theta_{eq}=109.5°$ for the bend. With this choice the probability distribution $\mathcal{P}_I(z_1,z_2,z_3)=\mathcal{P}_I(0,z_2-z_1,z_3-z_1)\equiv\mathcal{P}_I(z_2-z_1,z_3-z_1)$ is shown. This is the distribution that selects a window from the individual particle–surface interaction terms in an analogous manner to the rectangular patch of Fig. 5. The resulting potential is shown in Fig. 7.

appears as a square well centered at the value $z_1=z$. In this example the interaction term constrains the two particles to remain close together since it arises from a chemical bond. In panel B of Fig. 5 the bond has the effect of selecting the region of maximal overlap between the two surface-particle interactions. Without this restriction, the maximal overlap region is diluted by the overlap of the full particle-surface curves. This is precisely the difference between expressions (4) and (7) and results in the enhanced probability and corresponding deeper well depth for the bonded as opposed to the noninteracting particles, as shown in Fig. 4. Also shown in Fig. 4 is the case of a nonbonded Lennard-Jones interaction between the particles; this interaction is weak enough that it does not alter the effective center-of-mass potential from that of the noninteracting case. This completes the exposition of the two-particle coarse graining procedure; in the following section the extension to three particles is presented, along with a strategy for handling several particles in an efficient manner.

IV. THREE PARTICLES AND THE DIMENSIONALITY PROBLEM

A. Coarse graining three liquid particles

Three identical noninteracting particles have the joint distribution

$$\mathcal{P}(z_1,z_2,z_3)=e^{-\beta U(z_1)}e^{-\beta U(z_2)}e^{-\beta U(z_3)} \tag{8}$$

and the center-of-mass distribution

$$\mathcal{P}(z_1+z_2+z_3=3z)=\left(\frac{9}{2}z^2\right)^{-1}\int_0^{3z}dz_1\times\int_0^{3z-z_1}dz_2 e^{-\beta U(z_1)}e^{-\beta U(z_2)}e^{-\beta U(3z-z_1-z_2)}. \tag{9}$$

The corresponding potential is weak and diffuse.

When the particles interact the joint distribution becomes

$$\mathcal{P}(z_1,z_2,z_3)=e^{-\beta U(z_1)}e^{-\beta U(z_2)}e^{-\beta U(z_3)}\mathcal{P}_I(z_1,z_2,z_3) \tag{10}$$

and the center-of-mass distribution is

$$\mathcal{P}(z_1+z_2+z_3=3z)=\frac{\int_0^{3z}dz_1\int_0^{3z-z_1}dz_2 e^{-\beta U(z_1)}e^{-\beta U(z_2)}e^{-\beta U(3z-z_1-z_2)}\mathcal{P}_I(z_1,z_2,3z-z_1-z_2)}{\int_0^{3z}dz_1\int_0^{3z-z_1}dz_2\mathcal{P}_I(z_1,z_2,3z-z_1-z_2)}. \tag{11}$$

The interaction term only depends on the relative separation of the particles up to a normalization constant, $\mathcal{P}_I(z_1,z_2,3z-z_1-z_2)\mapsto\mathcal{P}_I(z_2-z_1,3z-2z_1-z_2)$. This two-dimensional distribution, shown in Fig. 6, selects a window from the individual surface-particle terms in analogy to the square-well one-dimensional window of Fig. 5. The potential corresponding to Eq. (11) is shown in Fig. 7.

B. Overcoming dimensionality

It is trivial to write down the many-particle version of the two- and three-particle expressions of Eqs. (7) and (11). However, with more than three particles the dimensionality of both the integration and the interaction probability $\mathcal{P}_I$ becomes unwieldy. This could be tackled with an appropriate Monte Carlo integration method. Instead, an iterative procedure will be used to reduce the calculation to a series of low-dimensional expressions. To illustrate this procedure, we reduce the two-dimensional calculation [three particles—Eq. (11)] to two sequential one-dimensional integrations. Considering only the first two particles we form the usual two-particle probability

$$\mathcal{P}_2(z)=\frac{\int_0^{2z}dz_1 e^{-\beta U(z_1)}e^{-\beta U(2z-z_1)}\mathcal{P}_I^{1,2}(2z-2z_1)}{\int_0^{2z}dz_1\mathcal{P}_I^{1,2}(2z-2z_1)}, \tag{12}$$

where $\mathcal{P}_I^{1,2}(\xi)$ is the probability of finding particles 1 and 2 a z-distance ξ apart. Now that we have coarse grained the first

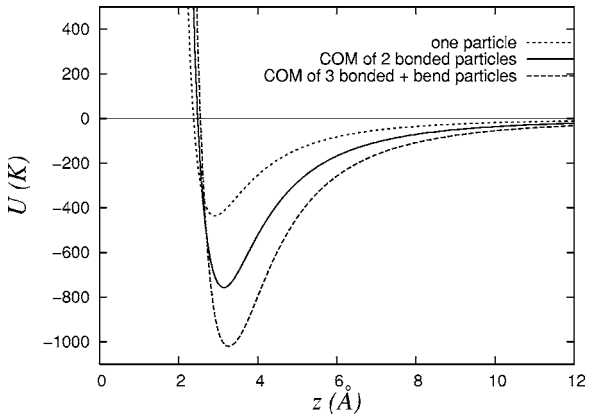

FIG. 7. Effective interaction potentials with the surface. Two of the curves in Fig. 4 are repeated here along with the three-particle unit of Fig. 6.

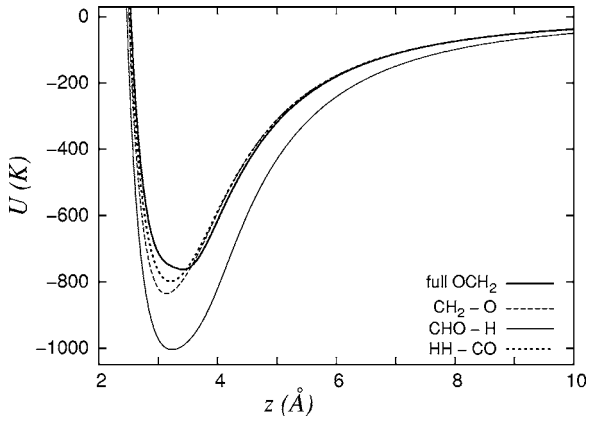

FIG. 8. The effective potential experienced by the center of mass of an $-O-CH_2-$ piece of poly(ethylene oxide) due to a graphite surface at $z=0$, and three approximations based on integrals of reduced dimensionality (see the text for details).

two particles, let us compute the two-particle probability arising from this newly coarse-grained particle and the third particle which we have not yet touched. We form

$$\frac{\int_0^{3z/2} dx \mathcal{P}_2(x) e^{-\beta U(3z-2x)} \mathcal{P}_I^{1/2,3}(3z-3x)}{\int_0^{3z/2} dx \mathcal{P}_I^{1/2,3}(3z-3x)}, \tag{13}$$

where $\mathcal{P}_I^{1/2,3}(\xi)$ is the probability of finding the center of mass of particles 1 and 2 a z-distance ξ from particle 3. The expression (13) is an approximation to Eq. (11) which only uses one-dimensional quantities. It is clear that $\mathcal{P}_I^{1,2}$ and $\mathcal{P}_I^{1/2,3}$ are marginal distributions of the full two-dimensional distribution $\mathcal{P}_I$. The exact relation is

$$\mathcal{P}_I^{1,2}(\xi) = \int du \mathcal{P}_I(\xi, u) \tag{14}$$

and

$$\mathcal{P}_I^{1/2,3}(\xi) = \int du \mathcal{P}_I(u, u/2 - \xi), \tag{15}$$

where, we wish to make clear, we are regarding $\mathcal{P}_I(u,v)$ as the probability of simultaneously finding particles 1 and 2 a z distance $u=z_2-z_1$ apart and particles 1 and 3 a z distance $v=z_3-z_1$ apart [see the discussion after Eq. (11)]. These relations can be used in an attempt to quantify the difference between expressions (13) and (11).

We now carry out a numerical example to illustrate the fidelity of the approximation—this will prove useful in Sec. V. We consider a $-CH_2-O-$ piece of poly(ethylene oxide). The full three-dimensional (four atom) expression is evaluated along with three approximations: (i) the CH_2 unit is coarse grained, and then this unit is combined with the oxygen atom; (ii) a CHO unit is coarse grained, and then this unit is combined with the remaining hydrogen atom; (iii) the HH and CO diatoms are coarse grained separately, and then these two units are combined. Figure 8 summarizes the data. Approximations (i) and (iii) are reasonable, while (ii) is in significant error, particularly in the tail of the potential. Scheme (i) is the natural reduction; the hydrogen atoms are combined with their associated heavy atom reminiscent of the united atom framework. Scheme (iii) is reasonable based on symmetry, while scheme (ii) is not natural and is not reasonable from either symmetry or chemical grounds. In Sec. V we will typically use scheme (i)—namely, the united atom approach. In this manner the error introduced by the dimensionality approximations is minimized.

V. DERIVATION OF A SPECIFIC FORCE FIELD

We are now in a position to apply the foregoing considerations to a real system consisting of molecules composed of many atoms of unequal masses. Specifically, we have derived the coarse grain liquid-graphite surface interactions for linear alkanes, poly(ethylene oxide), poly(ethylethylene) diblock copolymers, and 1,2-di-n-alkanoyl-*sn*-glycero-3-phosphocholine lipids.

The parameters in Eq. (2) are the number density of graphite, which is $\rho=0.113$ Å^{-3} (1.42 Å in-plane bond length and 3.4 Å interlayer spacing), and the site-site Lennard-Jones parameters of Eq. (1) which are tabulated in atomistic force fields such as CHARMM and OPLS: the graphite site is an sp^2 hybridized carbon atom typically labeled CA.

The potential [Eq. (2)] between graphite and each atom type in the liquid is constructed from these parameters. Since a coarse grain site typically contains three or more heavy atoms along with their accompanying hydrogen atoms,[4] we will use the approximation discussed in Sec. IV B to make the calculation feasible. Each heavy atom is combined with its accompanying hydrogen atoms into a united atom site. The united atom sites are combined in one or several steps to obtain the final coarse grain representation. The order in which this hierarchical grouping is performed affects the resulting potentials. The proposed order is physically motivated and the resulting error is small. If this is deemed unsatisfactory, the full dimensional expressions could be computed using an appropriate Monte Carlo integration scheme.

The interaction distributions $\mathcal{P}_I$ merit more discussion. We saw from Eq. (6) that the two-particle $\mathcal{P}_I$, which is one-dimensional, is best evaluated by first constructing the dis-

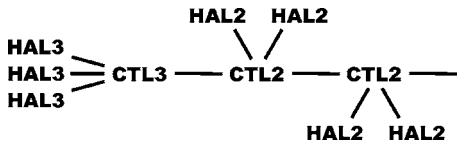

FIG. 9. Atoms comprising the coarse-grained terminal unit of dodecane. The CHARMM atom names are given.

tance distribution $\mathcal{P}_r$ and then changing variables to obtain the required z-distribution $\mathcal{P}_z$. For the three- and four-particle cases, it is difficult to relate the natural, internal, variables (bond distances, bond angles) to the Cartesian z variables. Furthermore, although it is an excellent approximation to directly convert the bond potential into a probability distribution in the two-particle case, this is not valid for the three- and four-particle cases because of the environment: for a CH_2 group in a linear alkane, the other CH_2 groups in the same molecule are coupled to it through bonds, bends, torsions, and nonbonded interactions, which perturbs the distribution away from that of CH_2 in isolation. As an example of a nonbonded effect, poly(ethylene oxide) adopts an all-*cis* conformation in vacuum, but an all-*trans* conformation is preferred in water. For these two reasons, it is best to build the distribution $\mathcal{P}_I$ directly from the z coordinates of a fully atomistic molecular-dynamics simulation. A problem arises, however, in practice. Since the simulation required to construct $\mathcal{P}_I$ does not include the surface, there is nothing special about the z direction—collecting the x or the y coordinate distribution must give the same result. But, for example, a hydrated lipid bilayer is not isotropic—the bilayer plane breaks the symmetry of the coordinates. The solution is to randomly rotate the reference frame to look at the simulation box from all possible angles. For a particle with coordinates (x_0,y_0,z_0), this is done by selecting a unit vector in three dimensions (see Appendix G.4 of Allen and Tildesley[23]), (a,b,c), and taking the z coordinate in the new reference frame as $ax_0+by_0+cz_0$. This has the double effect of symmetrizing the distribution and improving the sampling statistics. In practice this works extremely well; a few thousand random coordinate system rotations for each frame of simulation data is more than sufficient. The procedure outlined above is now explicitly carried out for the terminal coarse grain unit of dodecane and for the ester group of the DMPC phospholipid. The remaining coarse-grained interactions are computed in an analogous manner.

A. Terminal unit in dodecane

The connectivity and CHARMM atom names corresponding to the terminal coarse-grained unit of dodecane are shown in Fig. 9. We first form the CH_2 and CH_3 united atom sites. For CH_2, one of the hydrogen positions is eliminated as shown in Eq. (16), and the analogous expression to Eq. (11) is given in Eq. (17) where $\mathcal{P}_I$ is constructed as described above from an atomistic simulation of bulk dodecane:

$$m_C z_1 + m_H z_2 + m_H z_3 = m_{CH_2} z \Rightarrow z_3 = (m_{CH_2} z - m_C z_1 - m_H z_2)/m_H, \quad (16)$$

$$\mathcal{P}_{CH_2}(z) = \int_0^{m_{CH_2} z/m_C} dz_1 \int_0^{(m_{CH_2} z - m_C z_1)/m_H} dz_2 \times e^{-\beta U_{CTL2}(z_1)} e^{-\beta U_{HAL2}(z_2)} e^{-\beta U_{HAL2}(z_3)} \times \mathcal{P}_I(z_2 - z_1, z_3 - z_1). \quad (17)$$

In Eqs. (16) and (17) the masses are $m_C = 12.011$; $m_H = 1.008$; $m_{CH_2} = 14.027$. For CH_3, one of the hydrogen positions is eliminated as shown in Eq. (18), and the three-dimensional integral to compute $\mathcal{P}_{CH_3}$ is given as Eq. (19):

$$m_C z_1 + m_H(z_2 + z_3 + z_4) = m_{CH_3} z \Rightarrow z_4 = (m_{CH_3} z - m_C z_1 - m_H z_2 - m_H z_3)/m_H, \quad (18)$$

$$\mathcal{P}_{CH_3}(z) = \int_0^{m_{CH_3} z/m_C} dz_1 \int_0^{(m_{CH_3} z - m_C z_1)/m_H} dz_2 \times \int_0^{(m_{CH_3} z - m_C z_1 - m_H z_2)/m_H} dz_3 e^{-\beta U_{CTL3}(z_1)} \times e^{-\beta U_{HAL3}(z_2)} e^{-\beta U_{HAL3}(z_3)} e^{-\beta U_{HAL3}(z_4)} \times \mathcal{P}_I(z_2 - z_1, z_3 - z_1, z_4 - z_1). \quad (19)$$

In Eqs. (18) and (19) we define $m_{CH_3} = 15.035$. The united atoms are assembled into the terminal coarse grain unit of dodecane (see Fig. 9), as shown in Eqs. (20) and (21). The interaction probability $\mathcal{P}_I$ in Eq. (21) is constructed from the atomistic simulation by taking the coordinates z_i to be the centers of mass of the atoms involved in the united atom groups. We define $m_T = 43.089$:

$$m_{CH_3} z_1 + m_{CH_2} z_2 + m_{CH_2} z_3 = m_T z \Rightarrow z_3 = (m_T z - m_{CH_3} z_1 - m_{CH_2} z_2)/m_{CH_2}, \quad (20)$$

$$\mathcal{P}_T(z) = \int_0^{m_T z/m_{CH_3}} dz_1 \int_0^{(m_T z - m_{CH_3} z_1)/m_{CH_2}} dz_2 \times \mathcal{P}_{CH_3}(z_1) \mathcal{P}_{CH_2}(z_2) \mathcal{P}_{CH_2}(z_3) \mathcal{P}_I(z_2 - z_1, z_3 - z_1). \quad (21)$$

B. Ester group in DMPC lipid

The connectivity and CHARMM atom names corresponding to the coarse-grained ester group in DMPC are shown in Fig. 10. The CH_2 united atom unit is first constructed in an analogous fashion to the case for dodecane. This group is combined with the remaining three atoms in the ester site (see Fig. 10) to yield $\mathcal{P}_E$ via Eqs. (22) and (23). The potential is recovered via $U = -\beta^{-1} \log \mathcal{P}$. We define $m_O = 16.000$ and $m_E = 58.038$:

$$m_O z_1 + m_C z_2 + m_O z_3 + m_{CH_2} z_4 = m_E z \Rightarrow z_4 = (m_E z - m_O z_1 - m_C z_2 - m_O z_3)/m_{CH_2}, \quad (22)$$

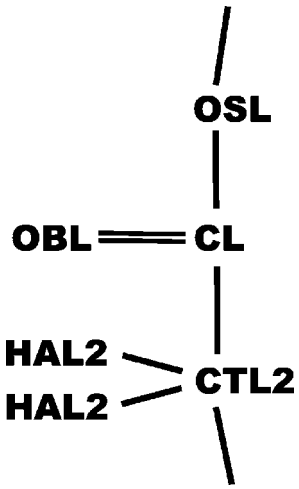

FIG. 10. Atoms comprising the coarse-grained ester unit of a phospholipid. The CHARMM atom names are given.

$$\mathcal{P}_E(z) = \int_0^{m_E z/m_O} dz_1 \int_0^{(m_E z - m_O z_1)/m_C} dz_2 \times \int_0^{(m_E z - m_O z_1 - m_C z_2)/m_O} dz_3 e^{-\beta U_{OSL}(z_1)} \times e^{-\beta U_{CL}(z_2)} e^{-\beta U_{OBL}(z_3)} \mathcal{P}_{CH_2}(z_4) \times \mathcal{P}_I(z_2 - z_1, z_3 - z_1, z_4 - z_1). \quad (23)$$

VI. WATER

The parametrization strategy detailed above is used for all solid-liquid interactions with the exception of water. Water in the existing CG framework consists of a Lennard-Jones particle which represents "a loose grouping of three water molecules."[13] We determine the water/graphite parameters by demanding that the CG water form a droplet on the CG graphite surface with a contact angle of $\theta_\infty = 86°$, using the methodology of Werder *et al.*[16] (see Fig. 1 of Werder *et al.*;[16] we use a droplet of 22 000 CG water particles corresponding to 66 000 water molecules). The resulting potential is $0.0338\epsilon\sigma^9 z^{-6} - 0.118\epsilon\sigma^6 z^{-3}$ with $\epsilon = 190$ K and $\sigma = 4$ Å. A snapshot from the parametrization simulation is shown in Fig. 11.

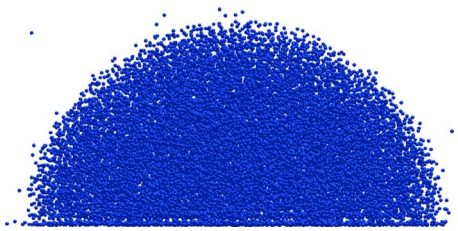

FIG. 11. A water droplet corresponding to 66 000 water molecules does not wet a graphite surface. The interaction strength between water and the surface was adjusted to bring the contact angle into agreement with experimental data.

VII. RETURN TO EXPLICIT GRAPHITE

In addition to the height-dependent implicit potential, we would like to have a site-site CG description to allow for arbitrary curved surface geometries, for example, a nanotube or an atomic force microscopy (AFM) tip. To recover such a description from the implicit representation, two of the integrals in Eq. (2) are performed to give

$$U(z) = \int_z^\infty dr \int_0^{2\pi} d\theta \int_{\pi - \cos^{-1}(z/r)}^{\pi} d\phi r^2 \sin\phi \rho u(r) = 2\pi\rho \int_z^\infty r u(r)[r - z] dr. \quad (24)$$

Two derivatives yield

$$u(\xi) = \frac{U''(\xi)}{2\pi\rho\xi}. \quad (25)$$

The number density ρ of sites enters into Eq. (24) in a trivial way: it simply appears as a constant multiplier. When we differentiate to recover the explicit potential, this factor must be specified [see Eq. (25)], and its value represents the level of coarse graining of the surface. For example, let us assume that we are presented with the surface potential given in Eq. (2). In recovering the explicit potential by the use of Eq. (25) let us assume we choose to use a value for ρ which is one-half of the value used in obtaining the surface potential in the first place. Namely, pretending we do not know that the value of ρ was used to get the expression in Eq. (2) because we are just given the function numerically, we happen to choose ρ in expression (25) as one-half of the density that went into yielding the surface potential $U(z)$. These choices yield the reconstructed explicit potential as $u(r) = 8\epsilon[(\sigma/r)^{12} - (\sigma/r)^6]$, which is exactly double the Lennard-Jones potential we began with [see Eq. (1)]. So what has happened? To recover the surface potential $U(z)$ with an assumed site density of only one-half of the actual value, we discover that we need twice the $u(r)$ potential. In other words, with only half as many sites (which can be thought of as a coarse graining by a factor of 2) we need a stronger potential to recover the same $U(z)$. This is perfectly reasonable and demonstrates that a site-site potential can be recovered in which the solid is coarse grained.

VIII. TEST: POLYETHYLENE ON GRAPHITE

As a test of the model we study a single molecule of $C_{350}H_{702}$ on graphite.[20] Although there are highly specialized force fields available for this system, we use the standard atomistic CHARMM description as our reference because we are doing a representative test, and for other molecules, such as surfactants, such highly specialized force fields do not exist.

The interaction between the polyethylene strand and the graphite surface is determined above [e.g., see Sec. V A for the CG description and Eq. (2) for the AA description]. However, for the CG polyethylene self-interaction we have two choices; the CG model of Shelley *et al.*[13] and the CG model of Nielsen *et al.*[8] In all three cases the polyethylene strand is

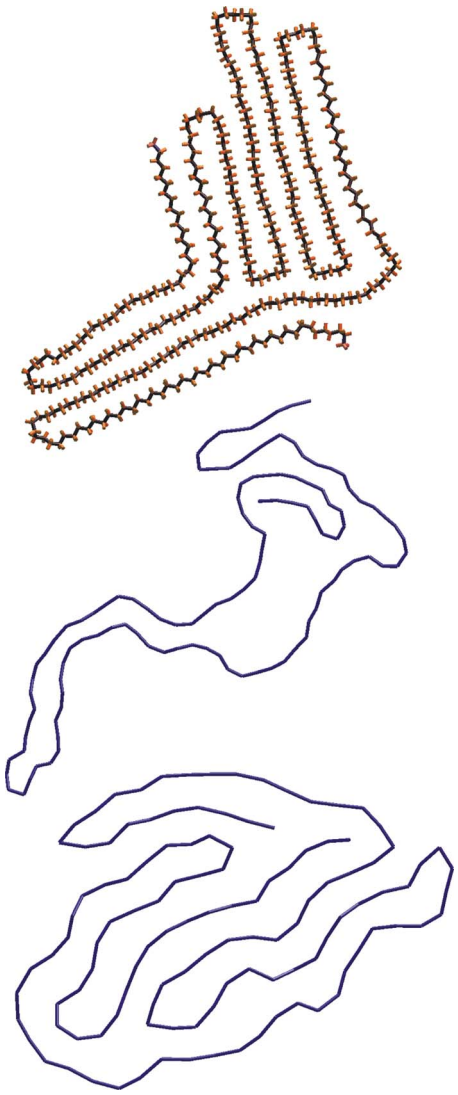

FIG. 12. Snapshots, in the *xy* plane, of $C_{350}H_{702}$ adsorbed onto a graphite surface. The top panel is for the fully atomistic CHARMM representation; the middle panel is for a coarse-grained representation with the polymer-polymer interactions given by the model of Shelley *et al.* (Ref. 13), and the bottom panel is for a coarse-grained representation with the polymer-polymer interactions given by the model of Nielsen *et al.* (Ref. 8).

strongly attracted to the graphite surface and loses almost all of its conformational freedom in the direction normal to the surface. The dynamics obey a two-dimensional self-avoiding walk in which polymer-polymer contacts are favorable. Representative snapshots of these systems are shown in Fig. 12, and the distribution of atoms vertically from the surface is shown in Fig. 13.

The atomistic data are first coarse grained in order to compare it to the CG simulation data by replacing each group of three consecutive carbon atoms, along with their associated hydrogens, with the center-of-mass location (see Ref. 8 for details). The two CG descriptions have almost identical vertical atom distributions but differ markedly in the number of self-contacts. As a measure of this, we calculated the two-dimensional mean-squared radius of gyration (R_g) for the polyethylene strands in the plane of the graphite sheet. The atomistic description and the CG description of Nielsen *et al.*[8] both favor conformations maximizing the

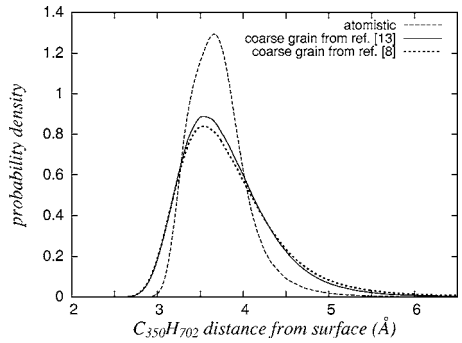

FIG. 13. Distribution of coarse grain units above the graphite surface for a polyethylene chain. The atomistic data have been coarse grained as described in the text. The two coarse grain descriptions have identical surface-polymer interactions but different polymer-polymer interactions.

number of contacts, and have an R_g of 550 and 500 Å^2, respectively. The CG description of Shelley *et al.*[13] prefers a more extended structure with some contacts, and has an R_g of 2200 Å^2. The description of Nielsen *et al.* is in excellent agreement with the atomistic data both in terms of the vertical distribution of atoms from the surface and in terms of the conformational entropy.

IX. CONCLUSIONS

The work presented in this paper describes a direct coarse graining procedure for solid-liquid interactions which is fundamentally different in nature from the coarse graining typically described in the literature. Coarse-grained simulations are not used to iteratively adjust parameters; rather the coarse-grained force field is built by using probability theory to combine atomistic interactions into effective center-of-mass interactions. This approach is possible because of the solid surface, which admits a description that is in some sense ultimately coarse grained: the entire surface can be replaced with a height-dependent implicit potential. Extensions of this work are proceeding in three directions. First, a hydrophilic surface is being considered by adding dipoles to the current description. Second, adsorption of surfactant on flat hydrophobic and hydrophilic surfaces is being studied. Lastly, the site-site description of Sec. VII is being used to study the solid-liquid interactions for other surface geometries.

ACKNOWLEDGMENTS

It is a pleasure to acknowledge and thank Bernd Ensing for stimulating conversations. This work was supported in part by Grant No. GM40712 from the National Institute of Health.

[1] S. O. Nielsen, C. F. Lopez, G. Srinivas, and M. L. Klein, J. Phys.: Condens. Matter **16**, R481 (2004).
[2] R. L. C. Akkermans and W. J. Briels, J. Chem. Phys. **114**, 1020 (2001).
[3] F. Müller-Plathe, ChemPhysChem **3**, 754 (2002).
[4] H. Fukunaga, J. Takimoto, and M. Doi, J. Chem. Phys. **116**, 8183 (2002).
[5] M. J. Stevens, J. H. Hoh, and T. B. Woolf, Phys. Rev. Lett. **91**, 188102 (2003).
[6] S. J. Marrink and A. E. Mark, J. Am. Chem. Soc. **125**, 11144 (2003).

[7] M. Muller, K. Katsov, and M. Schick, J. Polym. Sci., Part B: Polym. Phys. **41**, 1441 (2003).
[8] S. O. Nielsen, C. F. Lopez, G. Srinivas, and M. L. Klein, J. Chem. Phys. **119**, 7043 (2003).
[9] A. W. Adamson, *Physical Chemistry of Surfaces*, 5th ed. (Wiley, New York, 1990).
[10] M. J. Rosen, *Surfaces and Interfacial Phenomena*, 2nd ed. (Wiley, New York, 1989).
[11] H. N. Patrick, G. G. Warr, S. Manne, and I. A. Aksay, Langmuir **13**, 4349 (1997).
[12] M. F. Islam, E. Rojas, D. M. Bergey, A. T. Johnson, and A. G. Yodh, Nano Lett. **3**, 269 (2003).
[13] J. C. Shelley, M. Y. Shelley, R. C. Reeder, S. Bandyopadhyay, and M. L. Klein, J. Phys. Chem. B **105**, 4464 (2001).
[14] G. Srinivas, J. C. Shelley, S. O. Nielsen, D. E. Discher, and M. L. Klein, J. Phys. Chem. B **108**, 8153 (2004).
[15] S. O. Nielsen, G. Srinivas, C. F. Lopez, and M. L. Klein, Phys. Rev. Lett. **94**, 228301 (2005).
[16] T. Werder, J. H. Walther, R. L. Jaffe, T. Halicioglu, and P. Koumoutsakos, J. Phys. Chem. B **107**, 1345 (2003).
[17] T. L. Hill, *An Introduction to Statistical Thermodynamics* (Dover, New York, 1986).
[18] S. H. Lee and P. J. Rossky, J. Chem. Phys. **100**, 3334 (1994).
[19] J. C. Shelley and G. N. Patey, Mol. Phys. **88**, 385 (1996).
[20] R. Hentschke, B. L. Schürmann, and P. Rabe, J. Chem. Phys. **96**, 6213 (1992).
[21] M. Krishnan and S. Balasubramanian, Phys. Chem. Chem. Phys. **7**, 2044 (2005).
[22] A. D. Crowell, J. Chem. Phys. **22**, 1397 (1954).
[23] M. P. Allen and D. J. Tildesley, *Computer Simulations of Liquids* (Oxford University Press, Oxford, 1992).